

Current-induced spin polarization and spin-orbit torque in graphene

A. Dyrda¹ and J. Barnaś^{1,2}

¹Faculty of Physics, Adam Mickiewicz University, ul. Umultowska 85, 61-614 Poznań, Poland

²Institute of Molecular Physics, Polish Academy of Sciences, ul. M. Smoluchowskiego 17, 60-179 Poznań, Poland

(Dated: October 13, 2015)

Using the Green function formalism we calculate a current-induced spin polarization of weakly magnetized graphene with Rashba spin-orbit interaction. In a general case, all components of the current-induced spin polarization are nonzero, contrary to the nonmagnetic limit, where the only nonvanishing component of spin polarization is that in the graphene plane and normal to electric field. When the induced spin polarization is exchange-coupled to the magnetization, it exerts a spin-orbit torque on the latter. Using the Green function method we have derived some analytical formulas for the spin polarization and also determined the corresponding spin-orbit torque components. The analytical results are compared with those obtained numerically. Vertex corrections due to scattering on randomly distributed impurities is also calculated and shown to enhance the spin polarization calculated in the *bare bubble* approximation.

PACS numbers: 72.20.My, 72.80.Vp, 72.25.-b

I. INTRODUCTION

One of the main issues of the present-day spin electronics, that is of great importance for further development of high-density memory devices and magnetic random access memories, is effective manipulation of magnetization by a spin-polarized current. The general idea of switching and controlling orientation of a magnetic moment with electric current flowing through a system is based on coupling between the electron spin and magnetic moments. Two such interactions turned out to be especially useful – exchange interaction and spin-orbit coupling.

In a magnetically nonuniform system, the spin-polarized current generates a torque that is a consequence of: (i) exchange coupling between the conduction electrons and magnetization, and (ii) conservation of angular momentum in the system. The torque appears then as a result of the spin angular momentum transfer from a spin-polarized current (or pure spin current) to magnetic moments. Therefore, this torque is called spin-transfer torque.^{1,2} Such a torque leads, among others, to magnetic switching in spin valves and to domain wall displacements, as observed recently in many experiments. Moreover, these phenomena give a possibility to construct low-power non-volatile memory cells (STT-MRAM, racetrack memory), integrated circuits employing a logic-in-memory architecture as well as logic schemes processing information with spins.³

Another possibility to control orientation of magnetic moments is based on a spin torque that appears due to spin-orbit interaction in the system. The corresponding torque exerted on the magnetization is usually referred to as the spin-orbit torque, and appears also in a magnetically uniform system, like a single uniform layer. Physical mechanism of the spin-orbit torque is based on a nonequilibrium spin polarization of the system, which is induced by an external electric field (current) in the presence of spin-orbit interaction. Such a spin polarization was predicted long time ago in nonmagnetic systems, where an electric current flowing through the system with spin-orbit interaction was shown to induce not only the transverse spin-current^{4,5} (so-called spin Hall effect), but also

a spin-polarization of conduction electrons.^{6–11} In the case of two-dimensional electron gas with Rashba spin-orbit interaction, the induced spin polarization is in the plane of the electron gas and normal to the electric field. Such a nonequilibrium spin-polarization may be treated as an effective magnetic field, which may lead to reorientation of a magnetic moment, and also can modify or induce magnetic dynamics. The spin-orbit torque was analyzed in recent few years in many papers, mainly in metallic and semiconductor heterostructures.^{12–17} While the current-induced spin polarization, known also as the inverse spin-galvanic effect,¹⁸ is well known and was investigated theoretically as well as experimentally in the recent three decades, the role of geometric phase in this effect, and consequently in the spin-orbit torque, was invoked only very recently.^{19–21}

In this paper we consider the current-induced spin polarization and spin-orbit torque in graphene, which is assumed to be deposited on a substrate that ensures the presence of spin-orbit interaction of Rashba type²². We also assume that the graphene is magnetized, which may be either due to the magnetic proximity effect to a ferromagnetic substrate (or cover layer), or due to magnetic atoms (nanoparticles) on its surface.^{23–27} Coexistence of the Rashba spin-orbit interaction and proximity-induced magnetism in graphene was predicted theoretically and also observed experimentally.^{27–31} As the spin transfer torque in ferromagnetic graphene junctions was already considered theoretically (see e.g. Yokoyama and Linder³²), the problem of spin torques induced by spin-orbit interaction in graphene is rather unexplored.

It has been shown that the current-induced spin polarization in a defect-free nonmagnetic graphene with Rashba spin-orbit interaction is oriented in the graphene plane and is also normal to the current orientation. Moreover, sign of the spin-polarization depends on the chemical potential and also on the sign of the Rashba spin-orbit coupling parameter.³³ When the Fermi level passes through the Dirac points, the spin polarization becomes reversed. In this paper we show that the current-induced spin polarization in magnetic graphene has generally all three components. In the approximation linear with respect to the magnetization, one of these components is

equal to that in the case of a nonmagnetic graphene, i.e. it is proportional to the relaxation time. The leading terms in the other two components are independent of the relaxation time.

The paper is organized as follows. In Sec. 2 we describe the model and present a general formula describing current-induced spin polarization. Analytical formulas as well as numerical results for the current-induced spin polarization are presented in Sec. 3. Vertex correction is calculated in section 4, while the spin-orbit torque is described and discussed in Sec. 5. Summary and final conclusions are in Sec. 6.

II. MODEL AND METHOD

Transport properties of graphene close to the charge neutrality point are determined mainly by electrons in the vicinity of Dirac points. The corresponding effective-mass Hamiltonian, H_K^0 , which describes the low-energy electronic states in graphene around the K point of the Brillouin zone, can be written as a sum of three terms,³⁴

$$H_K^0 = H_0 + H_R + H_M. \quad (1)$$

The first term, H_0 , describes the low energy electronic states of pristine graphene, and can be written as a matrix in the pseudospin (sublattice) space,

$$H_0 = v \begin{pmatrix} 0 & (k_x - ik_y)\sigma_0 \\ (k_x + ik_y)\sigma_0 & 0 \end{pmatrix}, \quad (2)$$

where $v = \hbar v_F$, with v_F denoting the electron velocity in graphene, which is constant. The second term in Eq. (1) describes the Rashba spin-orbit interaction due to a substrate,

$$H_R = \lambda \begin{pmatrix} 0 & \sigma_y + i\sigma_x \\ \sigma_y - i\sigma_x & 0 \end{pmatrix}, \quad (3)$$

with λ being the Rashba spin-orbit coupling parameter. The last term of the Hamiltonian (1) represents the influence of an effective exchange field $\tilde{\mathbf{M}}$ created by a nonzero magnetization. Such a magnetization can appear in graphene, for instance, due to the proximity effect to a magnetic substrate. This term can be written in the form,

$$H_M = -\tilde{\mathbf{M}} \cdot \begin{pmatrix} \boldsymbol{\sigma} & 0 \\ 0 & \boldsymbol{\sigma} \end{pmatrix}, \quad (4)$$

where the exchange field $\tilde{\mathbf{M}}$ is measured in energy units. This field can be related to the magnetization \mathbf{M} and the local exchange interaction between the conduction electrons and magnetization in the two-dimensional graphene, $J_{\text{ex}}(\mathbf{r} - \mathbf{r}') = J_{\text{ex}} \delta(\mathbf{r} - \mathbf{r}')$, via the formula $\tilde{\mathbf{M}} = (J_{\text{ex}}/2g\mu_B)\mathbf{M}$. Here, g is the Lande factor ($g = 2$), μ_B is the Bohr magneton, while positive and negative J_{ex} (measured in the units of Jm^2) correspond to antiferromagnetic and ferromagnetic coupling, respectively. In the above equations, $\boldsymbol{\sigma}$ is the vector of Pauli matrices, $\boldsymbol{\sigma} = (\sigma_x, \sigma_y, \sigma_z)$, while the matrix σ_0 denotes the unit matrix in the spin space. Note that the so-called intrinsic spin-orbit interaction in graphene is very small and therefore it is neglected in our consideration. In a general case, the magnetization vector \mathbf{M} may be oriented arbitrarily in space, and

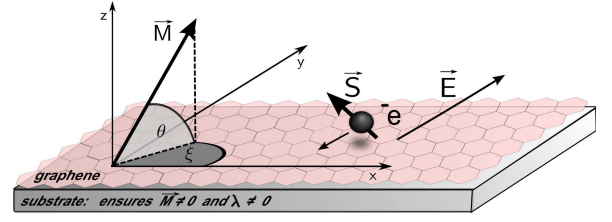


FIG. 1. (Color online) Schematic of the system under consideration. Graphene is on a substrate which assures a nonzero magnetization and also a spin-orbit interaction of Rashba type. Orientation of the magnetic moment \mathbf{M} is described by the angles θ and ξ . An external electric field is oriented along the axis y .

its orientation will be described by two spherical angles, θ and ξ , as indicated in Fig. 1. Moreover, the absolute magnitude of \mathbf{M} is assumed to be constant, $|\mathbf{M}| \equiv M = \text{const}$. Hamiltonian for the second non-equivalent Dirac point, K' , can be obtained from H_K by reversing sign of the wavevector component k_x and substitution $\sigma_y \rightarrow -\sigma_y$ in H_R .

In the lowest order with respect to the exchange field $\tilde{\mathbf{M}}$, the casual Green function corresponding to the Hamiltonian (1), $G_k^0 = \{[\varepsilon + \mu + i\delta \text{sign}(\varepsilon)] - H_K^0\}^{-1}$ has poles at $\varepsilon = E_n - \mu - i\delta \text{sign}(\varepsilon)$, where E_n ($n = 1-4$) are eigenvalues of the Hamiltonian (1) without the term H_M . These eigenvalues have the following form:

$$E_{1,2} = \mp\lambda - \sqrt{k^2v^2 + \lambda^2} \quad (5)$$

$$E_{3,4} = \mp\lambda + \sqrt{k^2v^2 + \lambda^2}, \quad (6)$$

where $E_{1,2}$ correspond to the valance bands, while $E_{3,4}$ describe the conduction bands. Note, the bands corresponding to $n = 2$ and $n = 3$ touch each other at the Dirac point ($k = 0$), while a gap equal to 4λ appears between the bands $n = 1$ and $n = 4$.

In the presence of a dynamical external electric field applied along the axis y , the total Hamiltonian for electrons near the K point takes the form

$$H = H_K^0 + H_K^A, \quad (7)$$

where the second term,

$$H_K^A = -e\hat{v}_y A_y(t) = -ie\frac{v}{\hbar} \begin{pmatrix} 0 & -\sigma_0 \\ \sigma_0 & 0 \end{pmatrix} A_y(t), \quad (8)$$

is the perturbation due to interaction with the time-dependent electromagnetic field represented by the vector potential $A_y(t) = A_y e^{-i\omega t}$. Here, e is the electron charge, \hat{v}_y is the y -component of the electron velocity operator, $\hat{v} = \partial H_K^0 / \partial \mathbf{k}$, whereas ω is the frequency of the dynamical field (later we will take the limit of $\omega \rightarrow 0$).

When an electric current flows in the system due to the electric field, electron spins become polarized as a result of the cooperation of the current and Rashba spin-orbit coupling. This nonequilibrium spin polarization of conduction electrons can be calculated (in the zero-temperature limit) using the following formula:

$$S_\alpha(t) = -i\text{Tr} \int \frac{d^2\mathbf{k}}{(2\pi)^2} \hat{S}_\alpha G_{\mathbf{k}}(t, t')|_{t'=t+0}, \quad (9)$$

where $G_{\mathbf{k}}(t, t')$ is the zero-temperature causal Green function corresponding to the total Hamiltonian H (see Eq. 7), and \hat{S}_α is the spin vertex function defined as

$$\hat{S}_\alpha = \frac{\hbar}{2} \begin{pmatrix} \sigma_\alpha & 0 \\ 0 & \sigma_\alpha \end{pmatrix}. \quad (10)$$

Upon Fourier transformation with respect to the time variables and expansion in a series with respect to the vector potential $A_y = -iE_y/\omega$, the expression (9) for the induced nonequilibrium spin density takes the form

$$S_\alpha(\omega) = \frac{eE_y}{\omega} \text{Tr} \int \frac{d^2\mathbf{k}}{(2\pi)^2} \int \frac{d\varepsilon}{2\pi} \hat{S}_\alpha G_{\mathbf{k}}^0(\varepsilon + \hbar\omega) \hat{v}_y G_{\mathbf{k}}^0(\varepsilon). \quad (11)$$

In the dc limit, $\omega \rightarrow 0$, the above formula leads to the following expression for the spin polarization:

$$S_\alpha = \frac{e}{2\pi} E_y \hbar \text{Tr} \int \frac{d^2\mathbf{k}}{(2\pi)^2} \hat{S}_\alpha G_{\mathbf{k}}^{0R} \hat{v}_y G_{\mathbf{k}}^{0A}, \quad (12)$$

where $G_{\mathbf{k}}^{0R(A)}$ is the retarded (advanced) Green function corresponding to the unperturbed Hamiltonian (1), taken at the Fermi level ($\varepsilon = 0$). Upon taking into account Eqs (10) and (12), and also including the contribution from the second Dirac point, the expression for the induced spin polarization acquires the form

$$S_\alpha = \frac{e\hbar^2}{2\pi} E_y \text{Tr} \int \frac{d^2\mathbf{k}}{(2\pi)^2} \begin{pmatrix} \sigma_\alpha & 0 \\ 0 & \sigma_\alpha \end{pmatrix} G_{\mathbf{k}}^{0R} \hat{v}_y G_{\mathbf{k}}^{0A}. \quad (13)$$

Based on this formula we calculate analytically as well as numerically the current-induced spin polarization, as described and discussed in the subsequent section.

III. CURRENT-INDUCED SPIN POLARIZATION

From the general formula (13) one finds the following expression for the α -th component of the spin polarization:

$$S_\alpha = \frac{e\hbar}{2\pi} E_y \int \frac{dkk}{(2\pi)^2} \frac{T_\alpha}{\prod_{n=1}^4 (\mu - E_n + i\Gamma)(\mu - E_n - i\Gamma)}, \quad (14)$$

where T_α is defined as

$$T_\alpha = \hbar \int_0^{2\pi} d\phi \text{Tr} \left[\begin{pmatrix} \sigma_\alpha & 0 \\ 0 & \sigma_\alpha \end{pmatrix} g_{\mathbf{k}}^{0R} \hat{v}_y g_{\mathbf{k}}^{0A} \right]. \quad (15)$$

Here, $g_{\mathbf{k}}^{0R(A)}$ is the nominator of the retarded (advanced) Green function, ϕ stands for the angle between the axis x and the wavevector \mathbf{k} , while $\Gamma = \hbar/2\tau$, where τ is the momentum relaxation time. The parameter Γ (or equivalently relaxation time τ) will be treated here as a phenomenological parameter, which effectively includes contributions due to momentum relaxation from various scattering processes (scattering on impurities, other structural defects, phonons, or electron-electron scattering). Note that Γ depends in general on the chemical potential μ and may be also different in the two Rashba subbands. However, when the Fermi level is in the two subbands, we assume for simplicity the same Γ for both of them.

Up to the terms linear in the exchange field \tilde{M} , the functions T_α ($\alpha = x, y, z$), see Eq. (15), can be written as follows:

$$T_x = 16\lambda\pi v\mu(k^4 v^4 - \mu^4 + 4\lambda^2 \mu^2), \quad (16a)$$

$$T_y = 64\pi v\lambda\tilde{M}\mu(k^2 v^2 - 2\lambda^2)\Gamma \sin\theta, \quad (16b)$$

$$T_z = -64\pi\lambda\tilde{M}v^3 k^2 \mu\Gamma \cos\theta \sin\xi. \quad (16c)$$

Note, the dependence on the orientation of \mathbf{M} is contained in the above expressions for T_y and T_z , while T_x is independent of \mathbf{M} . Equations (14) and (16) allow finding spin polarization in a general case, i.e. for an arbitrary relaxation time. However, some analytical expressions for all components of the spin polarization can be obtained in the limit of low impurity concentration, i.e. for long relaxation times ($\tau \rightarrow \infty$).

Consider first the x -component of the spin polarization. Combining Eq.(16a) with Eq.(14) and making the substitution $\sqrt{k^2 v^2 + \lambda^2} = \gamma$, one obtains

$$S_x = 8e\hbar E_y \lambda \mu \times \int_\lambda^\infty \frac{d\gamma\gamma}{v(2\pi)^2} \frac{(\gamma^2 - \lambda^2)^2 - \mu^4 + 4\lambda^2 \mu^2}{[(\mu + \lambda + \gamma)^2 + \Gamma^2][(\mu - \lambda + \gamma)^2 + \Gamma^2]} \times \frac{1}{[(\mu + \lambda - \gamma)^2 + \Gamma^2][(\mu - \lambda - \gamma)^2 + \Gamma^2]}. \quad (17)$$

From this formula follows that S_x is independent of \tilde{M} in the linear approximation with respect to the exchange field. For long relaxation times we get the same analytical formulas as those in the case of nonmagnetic graphene,³³ i.e.,

$$S_x = \frac{e}{4\pi} \frac{2\lambda \pm \mu}{v(\lambda \pm \mu)} \mu E_y \tau \quad (18)$$

for the Fermi level lying in the range $-2\lambda < \mu < 2\lambda$, and

$$S_x = \pm \frac{e}{4\pi} \frac{2\lambda}{v(\mu^2 - \lambda^2)} \mu^2 E_y \tau \quad (19)$$

for $|\mu| > 2\lambda$. In both above equations (as well as below), the upper and lower signs correspond to $\mu > 0$ and $\mu < 0$, respectively.

The spin polarization given by Eqs (18) and (19) is proportional to τ . However, one should bear in mind that these formulas were derived on the assumption of long τ . Therefore, one may expect some deviations from this formula when τ is finite and not too long. In Fig. 2(a) we show variation of the S_x component of spin polarization with the chemical potential μ and relaxation time τ , obtained by numerical integration of the formula (17). Figures 2b and 2c, in turn, present cross-sections of the density plots shown in Fig. 2(a) for constant values of τ and μ , respectively. The results obtained from the analytical formulas are compared in Figs 2(b) with those obtained by numerical integration of the formula (17). From this comparison follows that for τ of the order of 10^{-11} s or smaller, there are some deviations from the results given by the analytical formulas, though these deviations are not large. For τ of the order of 10^{-10} s or longer, numerical results match quite well those obtained from the analytical formulas. Since

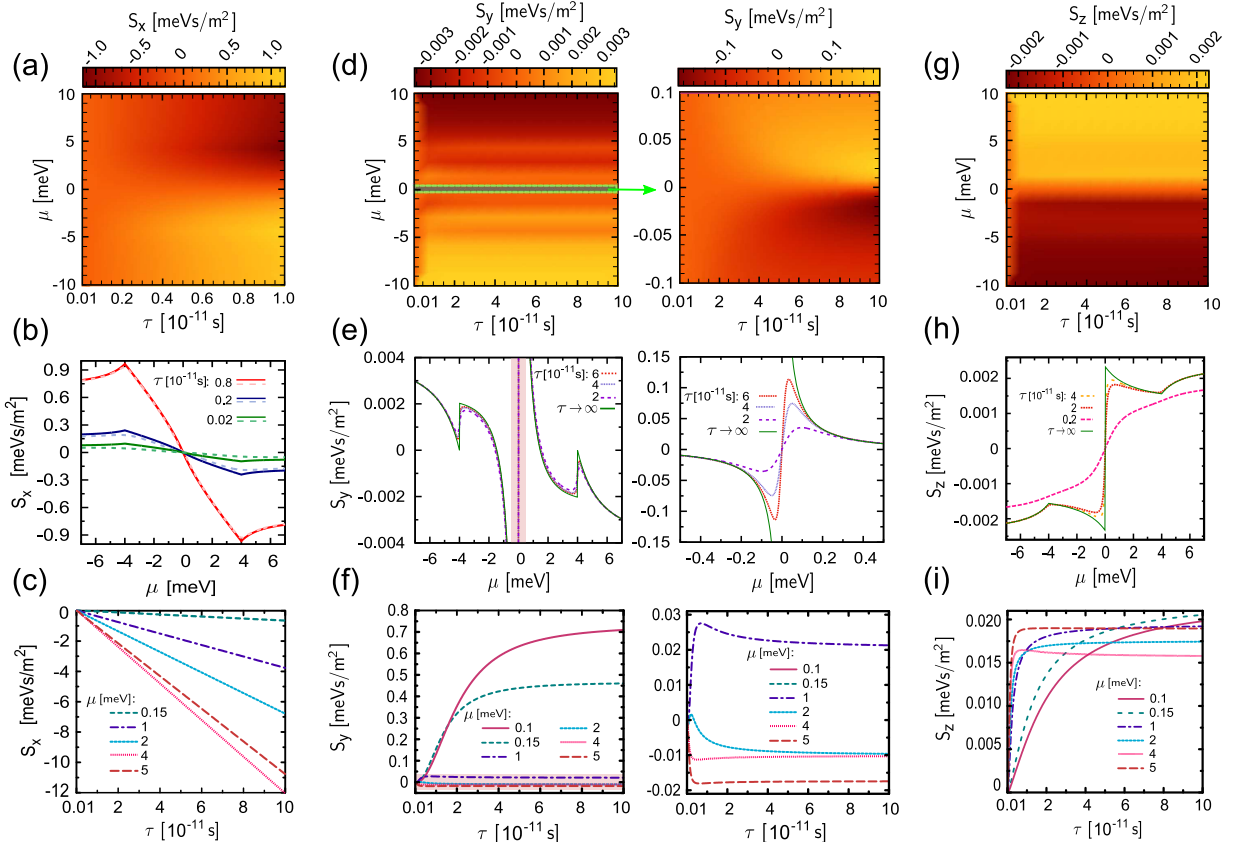


FIG. 2. (Color online) Spin polarization components induced by a current: (a,b,c) show the x -component, (d,e,f) show the y -component, whereas (g,h,i) show the z -component. The top panel (a,d,g) shows the spin polarization components as a function of chemical potential μ and relaxation time τ . The medium panel (b,e,h) shows the spin polarization components as a function of chemical potential μ for indicated values of τ , while the bottom panel (c,f,i) shows the polarization components as a function of τ for indicated values of μ . The right parts of (d,e,f) present the corresponding shaded regions in the left parts. The solid and dashed lines in (b) represent the results based on the analytical formulas and numerical integration, respectively. The curves for $\tau \rightarrow \infty$ in (e,h) correspond to analytical solutions. The other parameters are: $\lambda = 2$ meV, $E_y = 1$ V/cm, $\tilde{M} = 0.1$ meV, $\theta = \pi/3$, and $\xi = \pi/2$.

the S_x component is the same in magnetic and nonmagnetic limits (within the approximations used here), and in the non-magnetic limit it was considered and analyzed in Ref.[33], we will not discuss this component in more detail.

From Eqs (14) and (16b) one finds the y -component of the spin polarization in the following form:

$$S_y = 32eE_y\hbar\lambda\mu\tilde{M} \times \int_{\lambda}^{\infty} \frac{d\gamma\gamma}{v(2\pi)^2} \frac{(\gamma^2 - 3\lambda^2)\Gamma \sin\theta}{[(\mu + \lambda + \gamma)^2 + \Gamma^2][(\mu - \lambda + \gamma)^2 + \Gamma^2]} \times \frac{1}{[(\mu + \lambda - \gamma)^2 + \Gamma^2][(\mu - \lambda - \gamma)^2 + \Gamma^2]}. \quad (20)$$

In the limit of slow relaxation, $\Gamma \rightarrow 0$, the above formula leads to the following analytical results:

$$S_y = \pm \frac{e\hbar\tilde{M}}{4\pi\lambda} \sin\theta \frac{\mu(\mu \pm 2\lambda) - 2\lambda^2}{2v\mu(\mu \pm \lambda)} E_y \quad (21)$$

for $|\mu| < 2\lambda$, and

$$S_y = \pm \frac{e\hbar\tilde{M}}{4\pi\lambda} \sin\theta \frac{\mu^2 - 4\lambda^2}{v(\mu^2 - \lambda^2)} E_y \quad (22)$$

for $|\mu| > 2\lambda$.

Numerical results for the y -component of the current-induced spin polarization, obtained by numerical integration of the formula (20) are shown in Fig.2(d) as a function of chemical potential μ and relaxation time τ . Figures 2(e,f) present cross-sections of Fig.2(d). Figure 2(e) additionally shows the results obtained from analytical formulas, see the curves for $\tau \rightarrow \infty$. Right parts of Fig.2(d,e,f) present in more detail the corresponding shaded regions. Similarly as the x -component, S_y is antisymmetric with respect to reversal of the sign of Fermi energy, and its dependence on μ also reveals some steps at $\mu = \pm 2\lambda$. These steps are associated with the edges of the bands E_1 and E_4 . Moreover, when the Fermi level is at the Dirac point ($\mu = 0$), the analytical solution (21) for S_y becomes divergent. To understand origin of the divergency in the analytical solution for $\tau \rightarrow \infty$, one should note that the solution for the x -component is also infinite for $\tau \rightarrow \infty$, independently of μ . This clearly shows that the limit of $\tau \rightarrow \infty$ is not physical as the dissipation processes are necessary in order to stabilize a finite current-induced deviation of the system from equilibrium, and thus also a finite

current density and spin polarization. Therefore, in Fig.2(e) we compare the numerical results based on the corresponding analytical formulas with those obtained by numerical integration. This comparison clearly shows that the results obtained from the analytical formulas are roughly in agreement with those obtained from numerical integration, except the vicinity of $\mu = 0$, where the analytical solution diverges for $\mu \rightarrow 0$, while the numerical results based on Eq.(20) are then finite. Moreover, some discrepancy also occurs around $\mu = \pm 2\lambda$, but now the difference is finite and rather small. Thus, one should bear in mind that the analytical results (21) and (22) for the y -component have limited applicability range, and are not applicable for μ in the vicinity of the Dirac points.

The S_z component can be found from Eqs (14) and (16c) and acquires the form

$$S_z = -32eE_y\hbar\lambda\mu\tilde{M}\cos\theta\sin\xi \times \int_{-\lambda}^{\infty} \frac{d\gamma\gamma}{v(2\pi)^2} \frac{(\gamma^2 - \lambda^2)\Gamma}{[(\mu + \lambda + \gamma)^2 + \Gamma^2][(\mu - \lambda + \gamma)^2 + \Gamma^2]} \times \frac{1}{[(\mu + \lambda - \gamma)^2 + \Gamma^2][(\mu - \lambda - \gamma)^2 + \Gamma^2]}. \quad (23)$$

Similar calculations as those done for the y -component lead to the following analytical expressions in the limit of long relaxation time:

$$S_z = \mp \frac{e\hbar}{4\pi} \tilde{M}\lambda\cos\theta\sin\xi \frac{\mu \pm 2\lambda}{2v(\mu \pm \lambda)} E_y \quad (24)$$

for $\mu < 2\lambda$, and

$$S_z = \mp \frac{e\hbar}{4\pi} \frac{\tilde{M}}{\lambda} \cos\theta\sin\xi \frac{\mu^2 - 2\lambda^2}{v(\mu^2 - \lambda^2)} E_y \quad (25)$$

for $\mu > 2\lambda$.

In Fig.2(g) we present the z -component of the current-induced spin polarization, calculated as a function of the chemical potential and relaxation time by numerical integration of the formula (25). In turn, Figs.2(h,i) show cross-section of Fig.2(g). In Fig.2(h) we additionally compare the numerical results with those obtained from analytical solution. Now, the analytical solution is not divergent, see the curve for $\tau \rightarrow \infty$. When the relaxation time is sufficiently small, the numerical results obtained from Eq. (23) deviate from the results obtained on the basis of the analytical formulas. These deviations are rather small for $\tau \gtrsim 10^{-11}$ s, except the region near the zero chemical potential. However, the difference between the analytical and numerical results around $\mu = 0$ is now much less pronounced than it was in the case of the y -component (compare Fig.2(e) and Fig.2(h)). In turn, for $\tau \lesssim 10^{-11}$ s the deviations become remarkable in the whole range of the chemical potentials shown in Fig.2(h).

All the components of the spin polarization (S_x , S_y and S_z) vanish at $\mu = 0$ and are antisymmetric with respect to the sign reversal of the chemical potential. Numerical results presented above show that the spin polarization strongly depends on the Fermi level position. In the close vicinity of the Dirac points, the y -component of the spin polarization has pronounced peaks (positive above and negative below $\mu = 0$).

The other two components behave more regularly in this region. All three components exhibit some cusps (or dips) when μ is in the vicinity of $\mu = \pm 2\lambda$, i.e., when the Fermi level approaches the top edge of the band E_1 or bottom edge of the band E_4 . The spin polarization also remarkably depends on the Rashba parameter λ . This dependence reveals peculiarities of the corresponding electronic structure, and remarkably depends on the Rashba parameter. In numerical calculations we assumed the Rashba spin-orbit coupling parameter $\lambda = 2$ meV. Generally, this parameter depends on the substrate (or cover layer), and in real systems varies from a few to a few tens of meV, see eg. Refs [35–40].

IV. VERTEX CORRECTION

In the preceding section we have calculated spin polarization induced by electric field assuming effective relaxation time τ (or equivalently relaxation rate Γ). Both, τ and chemical potential were treated there as independent parameters. When considering a specific relaxation mechanism, these parameters usually are not independent. Since the dominant scattering processes are on impurities, we consider now this problem in more details. Assume the scattering potential created by randomly distributed weak short-range scatterers, which may be written as $V(\mathbf{r})_{s_0\sigma_0}$ with Gaussian correlations $\langle V(\mathbf{r})V(\mathbf{r}') \rangle = n_i V^2 \delta(\mathbf{r} - \mathbf{r}')$ (where s_0 and σ_0 and denote unit matrix in the pseudo-spin and spin subspace respectively).

Detailed calculation of the self energy due to scattering on the point-like impurities gives $\Gamma_{1,4} = \frac{n_i V^2}{2v^2} (|\mu| - \lambda)$ and $\Gamma_{2,3} = \frac{n_i V^2}{2v^2} (|\mu| + \lambda)$, where n_i is the impurity concentration while V is the impurity scattering potential. When $|\mu| \gg \lambda$, then indeed $\Gamma_{1,4} \simeq \Gamma_{2,3} \equiv \Gamma$. Otherwise, we take Γ as the average of $\Gamma_{1,4}$ and $\Gamma_{2,3}$, i.e. $\Gamma = \frac{n_i V^2}{2v^2} |\mu|$.

When calculating the impurity averaged conductivity, it is well known that non-crossing diagrams give an important contribution and renormalize the results obtained in the *bare bubble* approximation. Such a vertex renormalization is known to have a significant influence on the spin current induced via the spin Hall effect. In the case of two-dimensional electron gas with Rashba spin-orbit interaction it totally cancels the spin Hall conductivity obtained in the *bare bubble* approximation.^{41–44} However, this is not a general property and in other systems the vertex corrections can only reduce partly the spin Hall effect.^{45–47}

The problem of disorder in graphene was discussed in many papers.^{48–50} However, there is still a lack of information on the influence of disorder and impurities on spin-orbit driven phenomena in graphene. This problem was raised by Sinitsyn *et al.*⁵¹ and Gusynin *et al.*⁵² in the context of spin Hall and spin Nernst effect in the presence of intrinsic spin-orbit interaction in graphene and in the case of spin-independent random potential. In this case problem becomes simpler because one can reduce the model to 2×2 space. Such a simplification, however, is not possible in the presence of Rashba spin-orbit interaction.

In the weak scattering limit, the localization corrections are vanishingly small and therefore only noncrossing ladder diagrams are important. The summation over the ladder diagrams can be represented by the vertex corrections to the current-induced spin polarization. The renormalized spin vertex function is then given by the following equation:⁵³

$$\tilde{S}_\alpha = \hat{S}_\alpha + n_i V^2 \int \frac{d^2 \mathbf{k}}{(2\pi)^2} G_{\mathbf{k}}^A \tilde{S}_\alpha G_{\mathbf{k}}^R, \quad (26)$$

where \hat{S}_α is defined by Eq. (10). For the point-like scattering potential one can postulate the vertex function \tilde{S}_α in the form

$$\begin{aligned} \tilde{S}_\alpha = & a_\alpha \frac{\hbar}{2} \begin{pmatrix} \sigma_x & 0 \\ 0 & \sigma_x \end{pmatrix} + b_\alpha \frac{\hbar}{2} \begin{pmatrix} \sigma_y & 0 \\ 0 & \sigma_y \end{pmatrix} \\ & + c_\alpha \frac{\hbar}{2} \begin{pmatrix} \sigma_z & 0 \\ 0 & \sigma_z \end{pmatrix} + d_\alpha \frac{\hbar}{2} \begin{pmatrix} \sigma_0 & 0 \\ 0 & \sigma_0 \end{pmatrix}, \quad (27) \end{aligned}$$

for $\alpha = x, y, z$, where $a_\alpha, b_\alpha, c_\alpha$, and d_α are certain parameters to be determined. To find these parameters we multiply Eq. (26) by the matrix as specified below and take the trace,

$$\begin{aligned} \text{Tr} \left\{ \begin{pmatrix} \sigma_i & 0 \\ 0 & \sigma_i \end{pmatrix} \tilde{S}_\alpha \right\} = & \text{Tr} \left\{ \begin{pmatrix} \sigma_i & 0 \\ 0 & \sigma_i \end{pmatrix} \hat{S}_\alpha \right\} \\ & + n_i V^2 \int \frac{d^2 \mathbf{k}}{(2\pi)^2} \text{Tr} \left\{ \begin{pmatrix} \sigma_i & 0 \\ 0 & \sigma_i \end{pmatrix} G_{\mathbf{k}}^A \tilde{S}_\alpha G_{\mathbf{k}}^R \right\}, \quad (28) \end{aligned}$$

for $i = 0, x, y, z$. Taking into account Eq. (27), one finds then a set of equations for the coefficients $a_\alpha, b_\alpha, c_\alpha, d_\alpha$.

We recall that in this paper the exchange field due to proximity effect is assumed to be small, so the current-induced spin polarization is limited to the terms linear in the exchange field. Consequently, the vertex correction is also calculated in the lowest order appropriate to have spin polarization linear in M .

For $\alpha = x$ we find that:

$$b_x = c_x = d_x = 0, \quad (29)$$

$$a_x = \frac{1}{1 - n_i V^2 \mathcal{I}_x}, \quad (30)$$

where

$$\mathcal{I}_x = \int \frac{dkk}{2\pi} \frac{\chi_x(\mu, \Gamma)}{\prod_{n=1}^4 (\mu - E_n + i\Gamma)(\mu - E_n - i\Gamma)} \quad (31)$$

and

$$\begin{aligned} \chi_x(\mu, \Gamma) = & k^6 v^6 + k^4 v^4 (3\Gamma^2 - \mu^2) + (\Gamma^2 + \mu^2)^3 \\ & + 4(\Gamma^4 - \mu^4) \lambda^2 + k^2 v^2 (\Gamma^2 + \mu^2) (3\Gamma^2 - \mu^2 + 4\lambda^2) \\ & \approx (k^2 v^2 - \mu^2) (k^4 v^4 - \mu^4 + 4\mu^2 \lambda^2) \\ & + (3k^4 v^4 + 3\mu^4 + 2k^2 v^2 (\mu^2 + 2\lambda^2)) \Gamma^2. \quad (32) \end{aligned}$$

In the above equation, only terms up to the second order in Γ have been retained, while terms of higher order have been omitted.

For $\alpha = y$ we find the following coefficients:

$$a_y = c_y = d_y = 0, \quad (33)$$

$$b_y = a_x = \eta. \quad (34)$$

In turn, for $\alpha = z$ we find

$$a_z = b_z = d_z = 0, \quad (35)$$

$$c_z = \frac{1}{1 - n_i V^2 \mathcal{I}_z} = \zeta, \quad (36)$$

where

$$\mathcal{I}_z = \int \frac{dkk}{2\pi} \frac{\chi_z(\mu, \Gamma)}{\prod_{n=1}^4 (\mu - E_n + i\Gamma)(\mu - E_n - i\Gamma)} \quad (37)$$

and

$$\begin{aligned} \chi_z(\mu, \Gamma) = & k^6 v^6 + k^2 v^2 (3\Gamma^2 - \mu^2) (\Gamma^2 + \mu^2) \\ & + (\Gamma^2 + \mu^2)^3 + k^4 v^4 (3\Gamma^2 - \mu^2 - 2\lambda^2) \\ & + (\Gamma^2 + \mu^2) (2(\Gamma^2 - 3\mu^2) \lambda^2 + 8\lambda^4) \\ \approx & ((k^2 v^2 - \mu^2)^2 - 4\mu^2 \lambda^2) (k^2 v^2 + \mu^2 - 2\lambda^2) \\ & + (3k^4 v^4 + 2k^2 v^2 \mu^2 + 3\mu^4 - 4\mu^2 \lambda^2 + 8\lambda^4) \Gamma^2. \quad (38) \end{aligned}$$

Finally the renormalized spin-vertex functions are:

$$\tilde{S}_x = \frac{\hbar}{2} \eta \begin{pmatrix} \sigma_x & 0 \\ 0 & \sigma_x \end{pmatrix} \quad (39)$$

$$\tilde{S}_y = \frac{\hbar}{2} \eta \begin{pmatrix} \sigma_y & 0 \\ 0 & \sigma_y \end{pmatrix} \quad (40)$$

$$\tilde{S}_z = \frac{\hbar}{2} \zeta \begin{pmatrix} \sigma_z & 0 \\ 0 & \sigma_z \end{pmatrix} \quad (41)$$

This means that the results obtained in the *bare bubble* approximation should be multiplied only by a numerical factor to take into account the vertex corrections due to disorder. More specifically, the results for S_x and S_y should be multiplied by the factor η while those for S_z should be multiplied by ζ . The situation is significantly different from that found in the case of spin Hall effect. This is because transport phenomena and spin polarization are affected by scattering on impurities in remarkably different ways.

In Fig.3(a) we show the renormalization parameter η as a function of chemical potential and relaxation time. Now the relaxation time is connected with the chemical potential through the relation $\frac{\hbar}{\tau} = \frac{n_i V^2}{v^2} |\mu|$. A single point in the τ, μ space corresponds to a well defined value of $n_i V^2$. However, possible values of $n_i V^2$ have been limited in Fig.3 to $n_i V^2 < (n_i V^2)_{\max}$, where $(n_i V^2)_{\max}$ is a certain maximum value which is physically reasonable. The central white region is bounded by the condition $\hbar/\tau = (n_i V^2)_{\max} |\mu|/v^2$ and is excluded for the considered parameters. In Fig.3c, in turn, we show the parameter η as a function of the relaxation time and the ratio $n_i V^2 / (n_i V^2)_{\max}$. As one might expect, this figure shows that the normalization parameter η becomes reduced with decreasing $n_i V^2$. Figures 3(b) and 3(d) present cross-sections of Fig.3(a) and 3(c), respectively. The above described results for η show that the S_x and S_y components are remarkably renormalized by the vertex correction and are enhanced by a factor of the order of 2 (between 1 and 3).

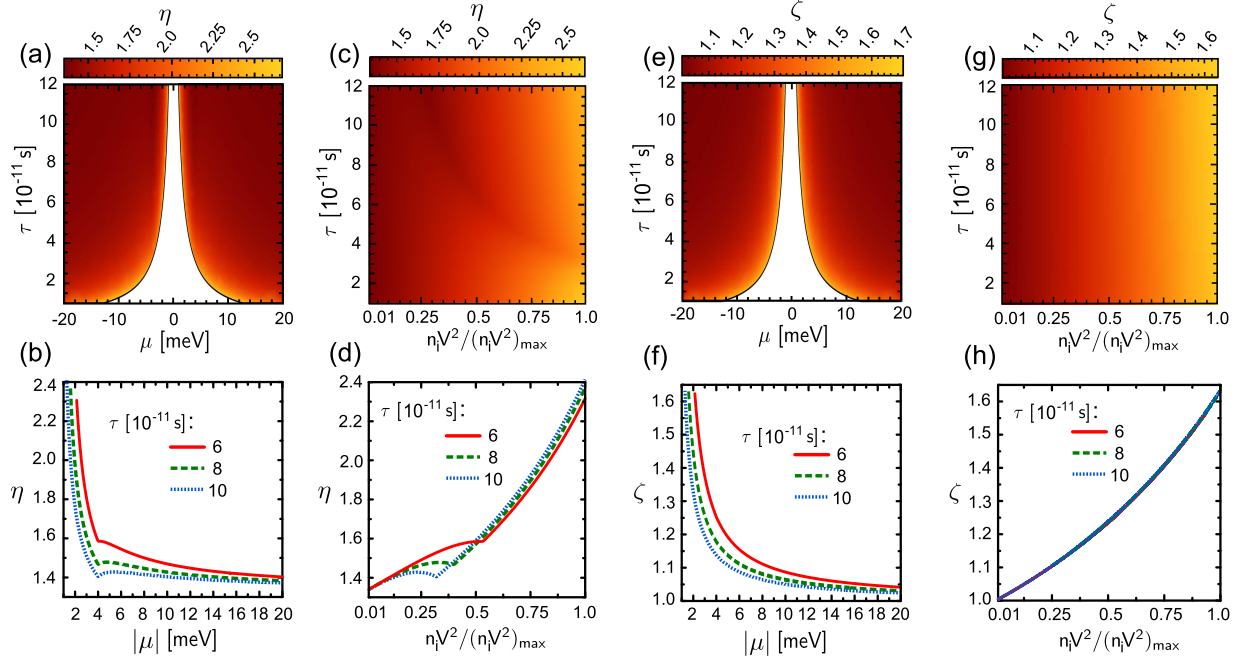


FIG. 3. (Color online) The parameter η as a function of the chemical potential and relaxation time (a) and as a function of relaxation time and $n_i V^2 / (n_i V^2)_{\max}$ (c). Figures (b) and (d) show η as a function of chemical potential μ (b) and $n_i V^2 / (n_i V^2)_{\max}$ (d) for indicated values the relaxation time. Figures (e)-(h) show the same variations as figures (a)-(d), but for the parameter ζ . The white regions in (a) and (e) are excluded for the assumed value of $(n_i V^2)_{\max} = 0.4 \times 10^{-2} (\text{eV} \cdot \text{nm})^2$. The other parameters are as in Fig.2.

This enhancement of the spin polarization is comparable to that found in the case of two-dimensional electron gas with Rashbe interaction.⁸ The parameter ζ , in turn, is shown in Fig.3e-f. It is of the same order of magnitude as the parameter η and depends on the chemical potential and relaxation time in a similar way, so we will not discuss it in more detail.

V. SPIN-ORBIT TORQUE

The current-induced spin polarization is exchange-coupled to the local magnetization \mathbf{M} and thus exerts a torque on \mathbf{M} . According to Eq.(4), energy of this interaction per unit area can be written as $E_{\text{ex}} = -(2/\hbar)\tilde{\mathbf{M}} \cdot \mathbf{S}$, where \mathbf{S} is the induced spin polarization. Taking into account the relation between $\tilde{\mathbf{M}}$ and \mathbf{M} , one finds the spin-orbit torque per unit area, $\boldsymbol{\tau}$, exerted on the magnetization (more precisely on the corresponding equilibrium spin polarization of the system) in the form

$$\boldsymbol{\tau} = \frac{2}{\hbar} \tilde{\mathbf{M}} \times \mathbf{S} = \frac{J_{\text{ex}}}{g\mu_B \hbar} \mathbf{M} \times \mathbf{S}. \quad (42)$$

Let us consider in more detail some specific situations as concerns relative orientation of the magnetization and electric field (current). Let us start with the situation when the magnetization \mathbf{M} is in the plane of the system and perpendicular to the current. This corresponds to $\theta = 0$ and $\xi = 0$ ($M_x = M \neq 0$ and $M_y = M_z = 0$). From the above general equation follows that the spin-orbit torque can be then written

in a general form as

$$\boldsymbol{\tau} = A(-\hat{j}M_x S_z + \hat{k}M_x S_y), \quad (43)$$

where \hat{i} , \hat{j} , and \hat{k} are unit vectors along the axes x , y and z , respectively, and we introduced the following abbreviation: $A = J_{\text{ex}}/g\mu_B \hbar$. Taking into account Eqs (21), (22), (24) and (25), one finds immediately that the spin-orbit torque in this geometry disappears because both S_y and S_z component of the spin polarization vanish.

Consider now the situation corresponding to $\theta = 0$ and $\xi = \pi/2$ ($M_y = M \neq 0$ and $M_x = M_z = 0$), i.e. the case when the magnetization is parallel to the electric current. From Eq.(42) follows that the spin-orbit torque has the following general form:

$$\boldsymbol{\tau} = A(\hat{i}M_y S_z - \hat{k}M_y S_x). \quad (44)$$

The S_z component is now nonzero, and thus both, S_z and S_x contribute to the torque in this geometry.

When $\theta = \pi/2$, namely $M_z = M \neq 0$ and $M_x = M_y = 0$, the magnetization is perpendicular to the graphene plane. The spin-orbit torque takes then the general form,

$$\boldsymbol{\tau} = A(-\hat{i}M_z S_y + \hat{j}M_z S_x). \quad (45)$$

Similarly as in the preceding situation, both S_y and S_x are nonzero and determine the torque.

In the last two cases the spin-orbit torque contains two components: linear term with respect to J_{ex} (proportional to S_x) and quadratic term in J_{ex} (proportional to S_z and S_y). The

spin orbit torque contains one component proportional to the relaxation time and another component whose the dominant part is independent on the relaxation time.

In a general case of arbitrary orientation of the magnetic moment, magnitude and character of the spin-orbit torque varies with the orientation of the magnetic moment. This is because two components of the current-induced spin polarization depend on the magnetization, while the third one is independent of \mathbf{M} . As a result the spin torque may have field-like and (anti)damping terms.

VI. SUMMARY

We have calculated current-induced spin polarization in graphene deposited on a ferromagnetic substrate, that ensures not only Rashba spin-orbit interaction but also a ferromagnetic moment in the graphene layer. To describe electronic spectrum of graphene we have used Kane Hamiltonian that describes low-energy states around the Dirac points. Using the zero-temperature Green functions formalism and linear response theory, we have derived analytical formulas for the spin polarization, up to the terms linear in M . Numerical results based on the analytical formulas have been compared with those obtained by numerical integration procedure. From this comparison we have formulated applicability conditions

of the analytical results. Significant deviations of the analytical results from those based on numerical integration have been found for relaxation times smaller than 10^{-10} s.

The nonequilibrium (current-induced) spin polarization exerts a torque on the magnetization *via* the exchange interaction. This torque contains a term which is proportional to the x -component of the induced spin polarization and therefore is proportional to the momentum relaxation time. The torque also includes a component whose main part is independent of the relaxation time.

The spin-orbit torque due to the interplay of external electric field and Rashba coupling at the interface between graphene and a magnetic layer can be used for instance to trigger magnetic dynamics and/or magnetic switching. Indeed, such a switching was observed experimentally in a recent paper by Wang *et al.*⁵⁴ However, instead of graphene they used MoS₂ – another two-dimensional honeycomb crystal.

ACKNOWLEDGMENTS

This work has been partially supported by the National Science Center in Poland as research project No. DEC-2013/10/M/ST3/00488 and by the Polish Ministry of Science and Higher Education through a research project 'Iventus Plus' in years 2015-2017 (project No. 0083/IP3/2015/73).

-
- ¹ A. Manchon, N. Ryzhanova, N. Strelkov, A. Vedyayev, and B. Dieny, *J. Phys.: Condens. Matter* **19**, 165212 (2007).
- ² D. C. Ralph, M. D. Stiles, *JMMM* **320**, 1190 (2008).
- ³ A. Brataas, A. D. Kent and H. Ohno, *Nature Materials* **11**, 372 (2012).
- ⁴ M. I. Dyakonov, V. I. Perel, *Pisma Z. Eksp. Teor. Fiz.* **13**, 657 (1971); *JETP Lett.* **13**, 467 (1971).
- ⁵ J. E. Hirsch, *Phys. Rev. Lett.* **83**, 1834 (1999).
- ⁶ M. I. Dyakonov and V. I. Perel, *Phys. Letters A* **35**, 459 (1971).
- ⁷ A. G. Aronov and Yu. B. Lynda-Geller, *JETP Lett* **50**, 431 (1989).
- ⁸ V. M. Edelstein, *Sol. State Communs.* **73**, 233 (1990).
- ⁹ A.G. Aronov, Y.B. Lyanda-Geller, G.E. Pikus, *Sov. Phys. JETP* **73**, 537 (1991).
- ¹⁰ E. L. Golub, E. I. Ivchenko, *Phys. Rev B* **84**, 115303 (2011).
- ¹¹ K. Shen, G. Vignale, R. Raimondi, *Phys. Rev. Lett.* **112**, 096601 (2014).
- ¹² A. Manchon and S. Zhang, *Phys. Rev. B* **78**, 212405 (2008).
- ¹³ A. Manchon and S. Zhang, *Phys. Rev. B* **79**, 094422 (2009).
- ¹⁴ A. Matos-Abiague, R. L. Rodriguez-Suarez, *Phys. Rev. B* **80**, 094424 (2009).
- ¹⁵ A. Manchon, arXiv:1204.4869v1 (2012).
- ¹⁶ P. Gambardella and I. M. Miron, *Phil. Trans. R. Soc. A* **369**, 3175 (2011).
- ¹⁷ K. Garello, I. M. Miron, C. O. Avci, F. Freimuth, Y. Mokrousov, S. Blugel, S. Auffret, O. Boulle, G. Gaudin, P. Gambardella, *Nature Nanotechnology* **8**, 587-593 (2013).
- ¹⁸ S. D. Ganichev, E. L. Ivchenko, V. V. Belkov, S. A. Tarasenko, M. Sollinger, D. Weiss, W. Wegscheider, W. Prettl, *Nature* **417**, 153 (2002).
- ¹⁹ H. Kurebayashi, J. Sinova, D. Fang, A.C. Irvine, J. Wunderlich, V. Novak, R.P. Campion, B.L. Gallagher, E.K. Vehstedt, L.P. Zarbo, K. Vyborny, A.J. Ferguson, and T. Jungwirth, *Nature Nanotechnology* **9**, 211 (2014).
- ²⁰ C. O. Avci, K. Garello, C. Nistor, S. Godey, B. Ballesteros, A. Mugarza, A. Barla, M. Valvidares, E. Pellegrin, A. Ghosh, I. M. Miron, O. Boulle, S. Auffret, G. Gaudin, P. Gambardella, *Phys. Rev. B* **89**, 214419 (2014).
- ²¹ H. Li, H. Gao, L. P. Zarbo, K. Vyborny, X. Wang, I. Garate, F. Dogan, A. Cejchan, J. Sinova, T. Jungwirth, A. Manchon, *Phys. Rev. B* **91**, 134402(2015).
- ²² Yu. S. Dedkov, M. Fonin, U. Rudiger, and C. Laubschat, *Phys. Rev. Lett.* **100**, 107602 (2008).
- ²³ T. Yokoyama, *Phys. Rev. B* **77**, 073413 (2008).
- ²⁴ H. Haugen, D. Huertas-Hernando, and A. Brataas, *Phys. Rev. B* **77**, 115406 (2008).
- ²⁵ Z. P. Niu, *J. Phys.: Condens. Matter* **23**, 435302 (2011).
- ²⁶ Z. P. Niu, *Phys. Lett. A* **378**, 73 (2014).
- ²⁷ P. Lazic, G. M. Sipahi, R. K. Kawakami, and Igor Zutic, *Phys. Rev. B* **90**, 085429 (2014).
- ²⁸ Z. Qiao, S. A. Yang, W. Feng, W.-K. Tse, J. Ding, Y. Yao, J. Wang, and Q. Niu, *Phys. Rev. B* **82**, 161414(R) (2010).
- ²⁹ Z. Qiao, W. Ren, H. Chen, L. Bellaiche, Z. Zhang, A. H. MacDonald, and Q. Niu, *Phys. Rev. Letters* **112**, 116404 (2014).
- ³⁰ Z. Wang, C. Tang, R. Sachs, Y. Barlas, and J. Shi, *Phys. Rev. Letters* **114**, 016603 (2015).
- ³¹ S. J. Gong, Z. Y. Li, Z. Q. Yang, Ch. Gong, Ch.-G. Duan and J. H. Chu *J. Appl. Phys.* **110**, 043704 (2011).
- ³² T. Yokoyama and J. Linder, *Phys. Rev. B* **83**, 081418(R) (2011).
- ³³ A. Dyrdał J. Barnaś, V. K. Dugaev, *Phys. Rev. B* **89**, 075422 (2014).
- ³⁴ C. L. Kane and E. J. Mele, *Phys. Rev. Lett.* **95** 226801 (2005).
- ³⁵ A. Varykhalov, D. Marchenko, M. R. Scholz, E. D. L. Rienks,

- T.K. Kim, G. Bihlmayer, J. Sanchez-Barriga, and O. Rader, Phys. Rev. Lett. **108**, 066804 (2012).
- ³⁶ D. Marchenko, A. Varykhalov, M.R. Scholz, G. Bihlmayer, E.I. Rashba, A. Rybkin, A.M. Shikin and O. Rader, Nature Commun. **3**, 1232 (2012).
- ³⁷ D. Marchenko, J. Sánchez-Barriga, M. R. Scholz, O. Rader, and A. Varykhalov, Phys. Rev. B **87**, 115426 (2013).
- ³⁸ J. Balakrishnan, G. K. W. Koon, M. Jaiswal, A. H. Castro Neto, and B. Özyilmaz, Nature Physics **9**, 284 (2013).
- ³⁹ J. Balakrishnan, G. K. W. Koon, A. Avsar, Y. Ho, J.H. Lee, M. Jaiswal, S.-J. Baeck, J-H. Ahn, A. Ferreira, M. A. Cazalilla, A. H. Castro Neto, and B. Özyilmaz, Nature Communications **5** 4748 (2014).
- ⁴⁰ A. Avsar, J. Y. Tan, T. Taychatanapat, J. Balakrishnan, G. K. W. Koon, Y. Yeo, J. Lahiri, A. Carvalho, A. S. Rodin, E. C. T. O'Farrell, G. Eda, A. H. Castro Neto, and B. Özyilmaz, Nature Communications **5**, 4875 (2014).
- ⁴¹ J. Inoue, G. E. W. Bauer, L. W. Molenkamp, Phys. Rev. B **70**, 041303 (2004).
- ⁴² R. Raimondi and P. Schwab, Phys. Rev. B **71**, 033311 (2005).
- ⁴³ O. V. Dimitrova, Phys. Rev. B **71**, 245327 (2005).
- ⁴⁴ O. Chalaev and D. Loss, Phys. Rev. B **71**, 245318 (2005).
- ⁴⁵ S. Murakami, Phys. Rev. B **69**, 241202(R) (2004).
- ⁴⁶ A. G. Malshukov and K. A. Chao, Phys. Rev. B **71**, 121308(R) (2005).
- ⁴⁷ P. L. Krotkov and S. Das Sarma, Phys. Rev. B **73**, 195307 (2006).
- ⁴⁸ E. McCann, K. Kechedzhi, V. Fal'ko, H. Suzuura, T. Ando, and B.L. Altshuler, Phys. Rev. Lett. **97**, 146805 (2006).
- ⁴⁹ P. M. Ostrovsky, I.V. Gornyi, A. D. Mirlin, Phys. Rev. B **74**, 235443 (2006).
- ⁵⁰ A. Pachoud, A. Ferreira, B. Ozyimaz, A.H. Castro Neto, Phys. Rev. B **90**, 035444 (2014).
- ⁵¹ N.A. Sinitsyn, J.E. Hill, H. Min, J. Sinova, and A. H. MacDonald, Phys. Rev. Lett. **97**, 106804 (2006).
- ⁵² V. P. Gusynin, S. G. Sharapov, and A. A. Varlamov, Phys. Rev. B **90**, 155107 (2014).
- ⁵³ G.D. Mahan, *Many Particle Physics*, (Kluwer Academic/Plenum Publishers, New York, 2000).
- ⁵⁴ W. Wang, A. Narayan, L. Tang, K. Dolui, Y. Liu, X. Yuan, Y. Jin, Y. Wu, I. Rungger, S. Sanvito, and F. Xiu, preprint arXiv:1502.06154.